# SAR-derived wind fields at the coastal region in the East/Japan Sea and relation to coastal upwelling

Tae-Sung Kim, Kyung-Ae Park, Xiaofeng Li & Sungwook Hong

Taylor & Francis
Taylor & Francis Group

# SAR-derived wind fields at the coastal region in the East/Japan Sea and relation to coastal upwelling

Tae-Sung Kim[a], Kyung-Ae Park[b,c]*, Xiaofeng Li[d], and Sungwook Hong[e]

[a]Department of Science Education, Seoul National University, Seoul, Korea; [b]Department of Earth Science Education, Seoul National University, Seoul, Korea; [c]Research Institute of Oceanography, Seoul National University, Seoul, Korea; [d]GST, National Environmental Satellite, Data, and Information Service (NESDIS), National Oceanic and Atmospheric Administration (NOAA), College Park 20740, USA; [e]Satellite Analysis Division, National Meteorological Satellite Center, Jincheon, Korea

The relationship between the modification of synthetic aperture radar (SAR) wind field and coastal upwelling was investigated using high-resolution wind fields from Advanced Land Observing Satellite (ALOS) Phased Array type L-band synthetic aperture radar (PALSAR) imagery and sea-surface temperature (SST) from National Oceanic and Atmospheric Administration/Advanced Very-High-Resolution Radiometer (NOAA/AVHRR) data. The retrieved SAR wind speeds seem to agree well with *in situ* buoy measurements with only a relatively small error of 0.7 m s$^{-1}$. The SAR wind fields retrieved from the east coast of Korea in August 2007 revealed a spatial distinction between near and offshore regions. Low wind speeds of less than 3 m s$^{-1}$ were associated with cold water regions with dominant coastal upwelling. Time series of *in situ* measurements of both wind speed and water temperature indicated that the upwelling was induced by the wind field. The low wind field from SAR was mainly induced by changes in atmospheric stability due to air–sea temperature differences. In addition, wind speed magnitude showed a positive correlation with the difference between SST and air temperature ($R^2$ = 0.63). The dependence of viscosity of water on radar backscattering at the present upwelling region was negligible since SAR data showed a relatively large backscattering attenuation to an SST ratio of 1.2 dB °C$^{-1}$. This study also addressed the important role of coastal upwelling on biological bloom under oligotrophic environments during summer.

## 1. Introduction

Coastal upwelling commonly occurs in regions where steady wind blows parallel to the coastline (Smith 1968). Worldwide, the west coast of the USA, the coasts of Peru and Chile, the northwest and southwest coasts of Africa, and the Iberian coast are all known to be upwelling-favourable places (Bakun 1990). Upwelling, as one of the most important coastal phenomena, leads to significant changes in water mass structure and primary production in the upper layer. Owing to its oceanographic impact and close relationship to human activity, several researchers have attempted to monitor these upwelling processes and identify their mechanisms (Van Camp et al. 1991; Nykjaer and Van Camp 1994;

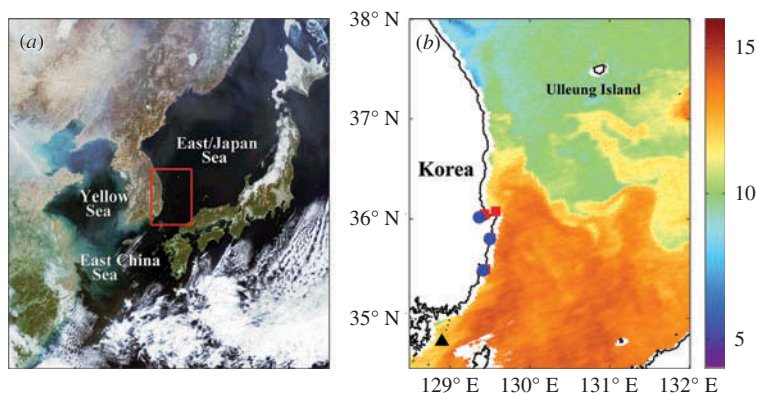*Corresponding author. Email: kapark@snu.ac.kr

Figure 1.  (a) GOCI RGB composite image of the seas around the Korea Peninsula on 5 April 2011 and (b) SSTs (°C) from NOAA/AVHRR of the study area on the same date, where the symbols rectangle (red), circle (blue), and triangle (black) indicate the locations of the NFRDI coastal station, AWS station of the Korea Meteorological Administration (KMA), and oceanic buoy station of KMA, respectively.

Thomas et al. 2001; Marín, Delgado, and Escribano 2003; Barth and Wheeler 2005; Santos, Kazmin, and Peliz 2005; Pradhan et al. 2006; Lathuilière, Echevin, and Lévy 2008).

The East/Japan Sea (EJS) has been known for unique rapid variabilities, leading to it being referred to as a miniature ocean (Kim et al. 2001). Its coastal regions have shown various oceanic phenomena and distinctive changes in sea-water temperatures due to upwelling, eddies, fronts, tides, topographic effects, and frequently passing atmospheric systems. The eastern coast of Korea is one of the places where seasonal coastal upwelling prevails in the Northwest Pacific including the Yellow Sea, the EJS, and the East China Sea (Figure 1).

Upwelling events frequently appear along the southeast coast of Korea in the EJS during the summertime (Lee 1983; Lee and Na 1985). Much of the previous literature has covered the appearance of cold water masses induced by coastal upwelling along the east coast of Korea and its responses (Lee, Kwon, and Hahn 1998; Suh, Jang, and Hwang 2001; Kim and Kim 2008; Lee, Ji, and Lee 2009; Kim et al. 2010; Lee 2011). Unlike the common upwelling events, an unprecedented coastal upwelling event occurred recently along the east coast of Korea over 37° N, which was much farther north than the usual upwelling sites (Park and Kim 2010). Park and Kim (2010) demonstrated that the existence of this unusual cold water mass was highly correlated with the behaviour of the North Pacific High and can be explained in terms of long-term large-scale variations due to global warming.

Basically, the occurrence of an upwelling can be recognized by a low sea-surface temperature (SST) with consistently blowing winds, high salinity, and high chlorophyll concentration (Flament, Armi, and Washburn 1985; Willson and Rees 2000). Satellite SST and scatterometer winds have been widely utilized to demonstrate wind-induced oceanic responses and their dynamics in the open ocean (McClain, Pietrafesa, and Yoder 1984; Bisagni and Sano 1993; Zheng et al. 1998; Fragiacomo and Parmiggiani 2002; Park, Cornillon, and Codiga 2006). However, the scatterometer data set has a limitation when interpreting small-scale phenomena at the coastal regions due to its low resolution of 25 km.

Figure 2 shows the coverage and observed wind field of QuikSCAT wind measurements of the seas around Korea. It is not possible to derive the spatial patterns of wind fields near the coast from scatterometer measurements. Contrarily, synthetic aperture radar
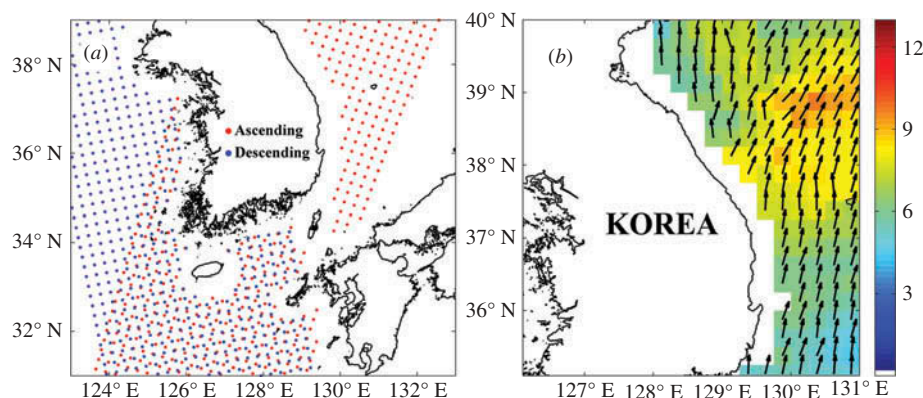
Figure 2. (*a*) Distributions of wind vector cells from QuikSCAT in the seas around Korea, where the red and blue circles represent those from ascending and descending modes for a day, respectively, and (*b*) an example of the wind field off the east coast of Korea from QuikSCAT, where the background colour and arrow indicate the magnitude of wind speed and the direction of wind vector, respectively.

(SAR) has the capability of high-resolution imaging, allowing for a detailed distribution of wind vectors to be retrieved with a spatial resolution of less than 1 km, even along the coastal regions, where scatterometers are inadequate. This makes it possible to identify the characteristics of wind field variations along coastal regions and enhance our understanding of fine-scale oceanic phenomena. Moreover, as an all-weather microwave sensor, SAR is capable of imaging the ocean surface irrespective of atmospheric clouds and moisture, with the exception of extreme events (Kim, Park, and Moon 2010). For these reasons, many oceanographers regard the SAR sensor as an innovate tool to investigate the spatial variability of oceanic phenomena and its mechanisms. During the upwelling period, coastal regions are usually covered with clouds and even severe fogs appear frequently. In this respect, the usage of SAR data can provide information regarding coastal wind fields with upwelling situations.

Some research has attempted to investigate the presence of coastal upwelling and its mechanisms using SAR data (Hsu, Mitnik, and Liu 1995; Clemente-Colon and Yan 1999; Clemente-Colón 2001; Svejkovsky and Shandley 2001; Li, Li, and He 2009). These studies demonstrated that upwelling regions are associated with low backscattering on SAR images by comparing SAR observations with SST measurements. Despite the applicability of SAR, upwelling investigations using SAR data have been very limited in general cases at the specific regions due to lack of *in situ* measurement and coincident thermal and other satellite observations. Hence, none of the studies have paid attention to utilizing SAR data for detection and analysis of coastal upwelling in the EJS.

In this study, we focused on the modification of SAR-derived coastal wind data in relation to upwelling in the east coast of Korea and investigated its mechanism using SAR data, *in situ* measurement, and other sensor observations. The objectives of this study are to derive high-resolution sea-surface wind field from SAR data, to assess the accuracy of SAR wind by comparing it with *in situ* measurements of sea-surface winds, to investigate the relationship between coastal upwelling and spatial distinction of SAR wind fields using satellite-observed SST, and to address the role of marine atmospheric boundary layer (MABL) stability on coastal winds.

## 2. Data

### 2.1. SAR data

To derive coastal winds from SAR images observed during upwelling events in 2007, we tried to collect SAR images such as ENVISAT ASAR, Radarsat, and TerraSAR-X during the upwelling period. However, there were no images to observe the study area then except for Advanced Land Observing Satellite (ALOS) Phased Array type L-band synthetic aperture radar (PALSAR) images. So, we used only ALOS PALSAR images in this study. Details of PALSAR images for this study are summarized in Table 1.

We utilized PALSAR images along the east coast of Korea from the summer of 2007. These PALSAR data at L-band (23.6 cm wavelength) with HH-polarization were obtained in ScanSAR mode with a swath of 370 km and a spatial resolution of 100 m. The looking angle of the PALSAR images ranges from 17.5° to 43.2°. The PALSAR images were acquired at 02:00 on 6 August 2007 and at 02:02 (UTC) on 26 August 2007, with the centres of the images being located at 128.97° E, 35.50° N, and 128.43° E, 35.51° N, respectively.

### 2.2. Other satellite data

High-resolution SST images from the National Oceanic and Atmospheric Administration (NOAA) Advanced Very High Resolution Radiometer (AVHRR) were utilized to investigate the spatial distribution of SST. We acquired the AVHRR data of NOAA-16, 17, and 18 from the Research Institute of Oceanography (RIO), Seoul National University (SNU), and derived SSTs using a split-window Multi-Channel SST (MCSST) algorithm (McClain, Pichel, and Walton 1985).

For the determination of wind direction, reanalysis data from the European Centre for Medium-range Weather Forecasts (ECMWF) were obtained. The reanalysis winds were near-surface winds at 10 m with a spatial resolution of $1.5° × 1.5°$. Time differences between the model winds and PALSAR images were within 2 hours.

In addition, Sea-viewing Wide Field-of-view Sensor (SeaWiFS) chlorophyll-*a* concentration data were used to investigate the biological impact of coastal upwelling. SeaWiFS observes approximately 90% of the ocean surface every 2 days with eight bands including six visible bands, which range from 412 to 670 nm, and two near-infrared (NIR) bands of 765 and 865 nm. We utilized the level-3 Standard Mapped Images (SMI) obtained from the NASA Goddard Space Flight Center (GSFC) Distributed Active

Table 1. Characteristics of SAR image data used in this study.

| Parameter | ALOS PALSAR Image | |
| --- | --- | --- |
| | Image A | Image B |
| Frequency (MHz) | 1270 (L-band) | |
| Polarization state | HH-polarized | |
| Swath width (km) × Azimuthal range (km) | 370 × 390 | |
| Resolution (m) | 100 × 100 | |
| Look angle (°) | 17.58° to 43.27° | 17.59° to 43.22° |
| Acquired time | 02h 00m 11s on 6 August 2007 (UTC) | 02h 02m 17s on 23 August 2007 (UTC) |
| Central location | 128.97° E, 35.50° N | 128.43° E, 35.51° N |

Table 2. Details of *in situ* measurement data used in this study.

|  | Ocean buoy | Ground-based AWS | Coastal station |
| --- | --- | --- | --- |
| Variables | Wind speed<br>Wind direction<br>Sea surface<br>temperature (SST)<br>Humidity | Wind speed<br>Wind direction<br>Air temperature | Air temperature<br>Sea surface<br>Temperature (SST) |
| Temporal resolution | 1 hour | 10 minutes | 1 day |
| Location | 128.90° E, 34.76° N | 129.50° E, 35.78° N<br>129.36° E, 36.01° N<br>129.43° E, 35.48° N | 129.43° E, 36.04° N<br>129.57° E, 36.07° N<br>129.51° E, 35.80° N<br>129.44° E, 35.49° N |
| Agency | Korea Meteorological<br>Administration<br>(KMA) | Korea Meteorological<br>Administration<br>(KMA) | National Fisheries Research<br>and Development Institute<br>(NFRDI) |

Archive Center (DAAC). The level-3 SeaWiFS chlorophyll-*a* concentration data have a spatial resolution of 9 km × 9 km and are composited of level-2 data for a day, 8 days, a month, or a year (Hooker et al. 1992; Campbell, Blaisdell, and Darzi 1995). Owing to lack of data, we used monthly composited SMI data.

### 2.3. In situ *measurements*

To assess the accuracy of SAR-derived wind fields and investigate the upwelling response, *in situ* measurements from a meteorological buoy station belonging to the Korea Meteorological Administration (KMA), as well as coastal stations of the National Fisheries Research and Development Institute (NFRDI), were used. Details of *in situ* measurement data set are summarized in Table 2. While satellite-derived wind speeds were referenced to a height of 10 m, the wind data of the KMA buoy were measured at less than 10 m. For precise comparison with SAR winds, the measured wind speeds of the buoy were converted to 10 m neutral wind using a wind profile model, which includes air–sea stability effects (Brown and Liu 1982; Businger and Shaw 1984; Liu 1984; Kara, Wallcraft, and Bourassa 2008). Since the oceanic buoy stations were far from the coastal regions where upwelling events occurred, we also relied upon wind measurements from ground-based automatic weather stations (AWSs) of the KMA, which were located close to the upwelling regions.

### 3. Methods

### 3.1. *SAR wind retrieval*

Figure 3 presents the schematic flow chart of SAR wind retrieval from PALSAR images. Before applying the SAR wind-retrieval algorithm, SAR data were preprocessed to extract the normalized radar cross section (NRCS), incidence angles, and ancillary information such as the geolocation of pixels and radiometric parameters. For the PALSAR level 1.5 data, NRCS values were derived from a pixel value (digital number, DN) according to the following formula:
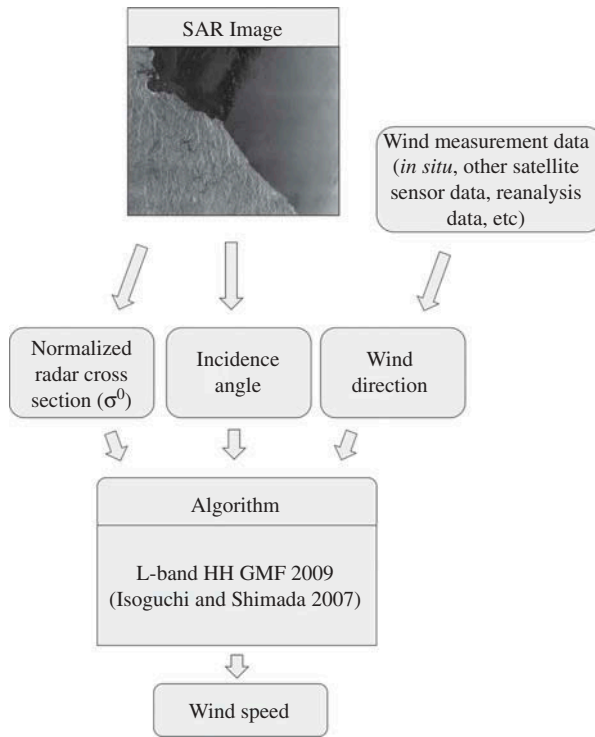
Figure 3.   Flow chart for sea-surface wind retrieval from L-band PALSAR data.

$$\text{NRCS} = 10 \log_{10}\langle \text{DN}^2 \rangle + \text{CF}, \tag{1}$$

where < > indicates the ensemble averaging of a pixel value and CF is a calibration factor. In the case of the PALSAR data used in this study, the calibration factor CF was given a value of −83 dB.

Figure 4 shows the distributions of the calculated NRCS from the PALSAR images. The value of NRCS in the ocean ranged from −25 to −3 dB and the mean of the values for
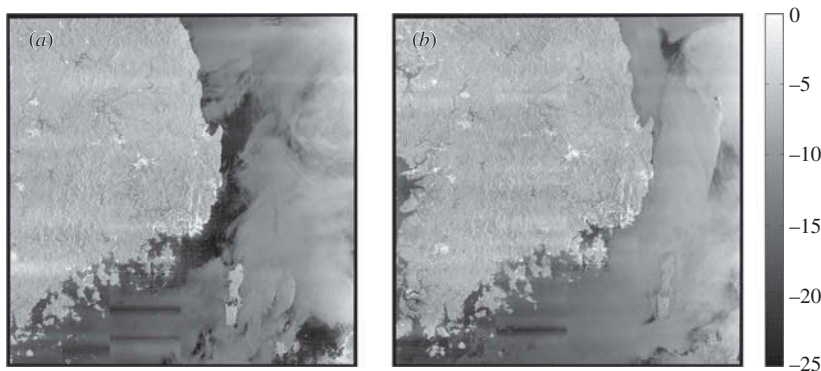


Figure 4.   The normalized radar cross-section images of PALSAR acquired on (a) 6 August 2007 and (b) 23 August 2007.

the entire data set amounted to −12.9 dB. The right part of the image, which was apart from the coast, showed higher values of about −7 dB whereas the middle parts of the image along the coastline showed a significantly lower value of about −19 dB. These features were associated with oceanic phenomena at the sea surface.

The SAR wind-retrieval model requires the input of wind directions prior to the estimation of wind speed. If wind-induced streaks are apparent on the image, then wind direction can be directly estimated from the SAR image using 2-D Fourier transform spectrum analysis (Wackerman et al. 1996; Vachon and Dobson 2000). Otherwise, the directions must be obtained from other external data such as *in situ* buoy measurements, scatterometer wind data, or numerical model products. In this study, wind directions were obtained from ECMWF reanalysis wind data sets owing to the lack of streaks in Figure 4.

To derive wind speed from SAR data, the model functions were used by considering NRCS and wind speed, relative wind direction, incidence angle, and polarization state. We used the robust L-band SAR geophysical model function (GMF) developed by Isoguchi and Shimada (2009) that has been widely used for L-band SAR wind retrieval (Leite et al. 2010; Isoguchi, Shimada, and Kawamura 2011; Kim et al. 2012).

The L-band HH GMF algorithm has been developed by comparison of the PALSAR observations with ASCAT winds, ECMWF reanalysis data, and National Data Buoy Centre (NDBC) measurements. The functional form of relationship between NRCS and wind vector is as follows:

$$
\begin{aligned}
\sigma_0 &= A_0(v,\theta)(1 + A_1(v,\theta)\cos\Phi + A_2(v,\theta)\cos2\Phi), \\
A_0 &= 10^{(a_0 + a_1 W + a_2 W^2 + a_3 W^3)/10}, \\
A_1 &= c_{13} + c_{14}x + c_{15}x^2 + (c_{16} + c_{17}x + c_{18}x^2)v, \\
A_2 &= \frac{b_0 + b_1 v + b_2 v^2}{1 + \exp(b_3 + b_4 v)},
\end{aligned}
\tag{2}
$$

where $\sigma_0$ is the NRCS, $v$ is the wind speed in 10 m height, $\theta$ is the incidence angle, and $\Phi$ is the direction of viewing relative to the wind direction, which is $\Phi = 0°$ when viewing upwind. The $A_n$ and $B_n$ are functions of the wind speed term $W = 10\log_{10}v$ and the incidence angle term $x = (\theta - 30°)/15°$. The coefficients $C_n$ are derived from the matchup data set.

### 3.2. Noise reduction

As shown in Figure 4, the PALSAR images off the east coast of Korea include some band-like noises. These noises have been detected worldwide. The band-like noise patterns were reported to have originated from the interference signals of the ground radars so that the degraded components of SAR raw data appear on the image (Shimada et al. 1999), although the exact causes of the noises have yet to be clarified.

The locations of the noise patterns were distributed randomly, but it had the shape of a kilometre-scale thick band and relatively high uniformity of NRCS values along the range direction. Thus, it is assumed that NRCS values corresponding to the noise can be extracted by abrupt discontinuity in the azimuthal and range directions. Figure 5(*a*) indicates an example of the image with band-like noise patterns. We extracted the noise from the image using spectral analysis, deriving uncorrelated signals from the neighbouring signals of the range direction (Figure 5(*b*)). In turn, as shown in Figure 5(*c*), the
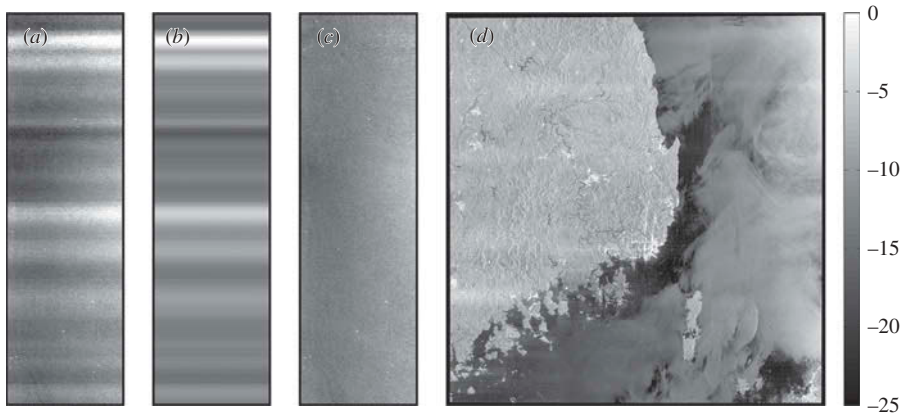
Figure 5. An example of (*a*) band-like noises on ALOS PALSAR image, (*b*) extracted noises from (*a*) using the spectral analysis, (*c*) retrieved normalized radar cross-section (NRCS) without noise patterns by subtracting (*b*) from (*a*), and (*d*) the NRCS image of Figure 4(*a*) after noise reduction procedure.

NRCS values without noise patterns were retrieved by subtracting them from the original image. Figure 5(*d*) demonstrates the NRCS image of Figure 4(*a*) after the noise reduction procedure. Although the staircase phenomena still appeared weakly, most of the band-like noises were significantly diminished, and the genuine structure of the coastal region was preserved. The noise-reduced images were used for the calculation of SAR wind fields.

### 3.3. Conversion of wind speed to the equivalent neutral wind at 10 m

In general, the satellite-based wind measurements are derived by assuming the neutral atmospheric stratification at a height of 10 m (Geernaert and Katsaros 1986). *In situ* buoy wind data, however, were measured at 6 m, requiring it to be converted to the equivalent wind speed at 10 m. Several algorithms for the adjustment of wind speed at an observed height to the standard height of 10 m have been developed, such as the Liu-Katsaros-Businger (LKB) model (Liu, Katsaros, and Businger 1979; Liu and Tang 1996), the logarithmically varying profile model (Peixoto and Oort 1992), and the Bourassa-Vincent-Wood (BVW) model (Bourassa, Vincent, and Wood 1999). Among these algorithms, we applied the LKB model to obtain the 10 m wind speed.

The LKB model was designed to calculate the height-adjusted wind speed using an observed wind speed and ancillary parameters such as air temperature, humidity, and SST. The functional form of the LKB model is expressed as follows:

$$(U - U_s)/U^* = (\ln(z/z_0) - \psi_u)/k, \tag{3}$$

where $U$ and $U_s$ indicate the wind speed at 10 m and at the sea surface, respectively. The values of $z$ and $z_0$ are the referenced and observed height, respectively, and $k$ is the von Karman constant. We used a $k$ value of 0.4, which is from Paulson (1970). The friction velocity at sea surface $U^*$ was given by the relation between wind stress and air density.

Under unstable conditions, the Businger-Dyer model (Businger et al. 1971; Dyer 1974) gives the following stability parameter function $\psi_u$:

$$\psi_u = 2\ln((X+1)/2) + \ln\big((X^2+1)/2\big) - 2\tan^{-1}(X) + \pi/2, \tag{4}$$

where $X = (1 + a_u\xi)^{1/4}$ and $\xi = z/L$. The coefficient $a_u$ was given a value of 10 and the Obukhov length $L$ was derived using the potential temperature $T$ and specific humidity $Q$ (Liu and Tang 1996). More details are available in Liu and Tang (1996).

## 4. Results

### 4.1. Spatial distinction of coastal wind

Figures 6(a) and (b) show the distribution of wind speeds retrieved from PALSAR data using the L-band HH GMF algorithm along the east coast of Korea on 6 and 23 August 2007, respectively. On 6 August 2007, the mean wind speed in the study area was 4.5 m s$^{-1}$. Moderate southerly winds of around 5 m s$^{-1}$ were apparent off the east coast of Korea and relatively strong southeasterly winds ranging from 6 to 10 m s$^{-1}$ appeared off the southern coast. By contrast, low winds of less than 3 m s$^{-1}$ were dominantly distributed along the east coast. On the other hand, the spatial distribution of the SAR wind field on 23 August 2007 showed a relatively uniform pattern overall with a prevailing strong southwesterly wind, except for in the upper right part of the image where a significant low wind patch appeared, which stretched from the coast of cape Homi (red dot on Figure 6) at 36° N to northeastward corresponding to the wind direction. The mean of wind speeds in Figure 6(b) indicated a value of 6.3 m s$^{-1}$ whereas the wind speeds of the patch were less than 2.5 m s$^{-1}$. The retrieved SAR wind speed coincided well with buoy measurements (128.90° E, 34.76° N) by a difference of 0.7 m s$^{-1}$, which were 3.0 m s$^{-1}$ for the SAR wind and 2.3 m s$^{-1}$ for the buoy wind, respectively.
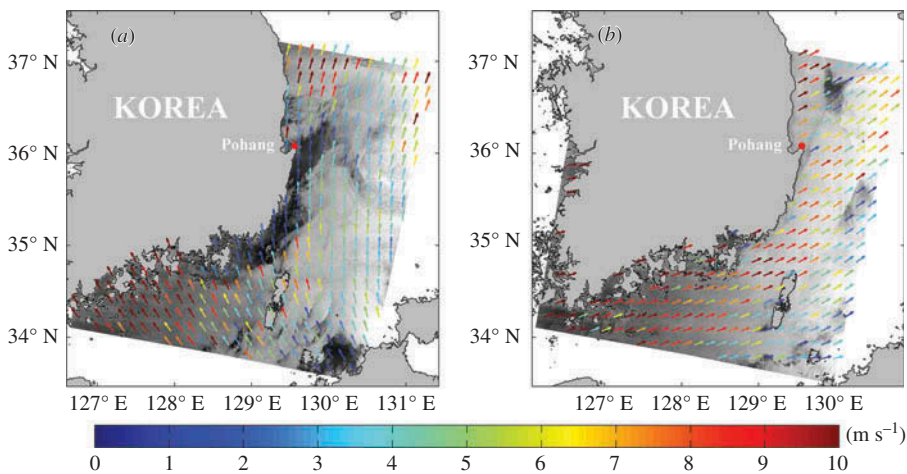


Figure 6. Distributions of wind vectors retrieved from the PALSAR imagery at (a) 02h 00m (UTC) on 6 August 2007 and (b) 02h 02m on 23 August 2007, where the colour and the arrows of vectors indicate the magnitude and direction of wind vectors, respectively, where the red dot indicates the location of Cape Homi.
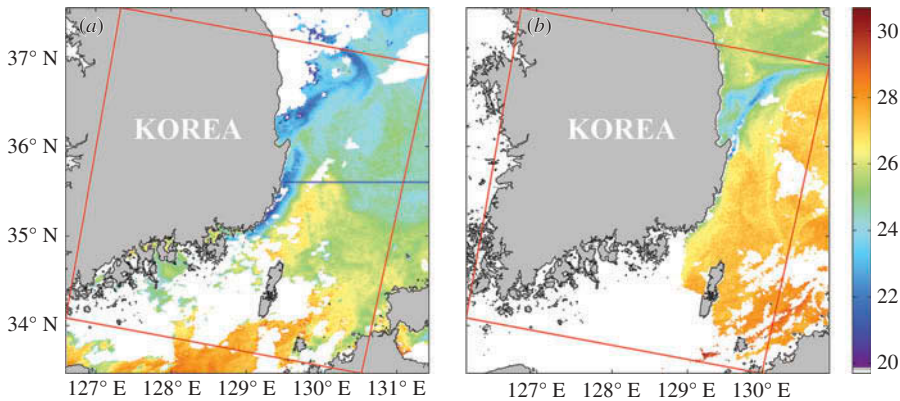
Figure 7.    Distributions of sea-surface temperature (ºC) from NOAA AVHRR at (*a*) 12h 22m (UTC) on 4 August 2007 and (*b*) 06h 38m on 23 August 2007, where the red box indicates the boundary of ALOS PALSAR images and the blue line represents the section for the comparison with sea-surface temperature.

### 4.2.    Wind and SST conditions during the upwelling

To investigate the causes of spatial distinction of SAR wind fields at the coastal regions, we analysed the distributions of SST and wind conditions during upwelling events. Figures 7(*a*) and (*b*) present the spatial distribution of SST from NOAA AVHRR on 4 August 2007 and 23 August 2007, respectively. On 4 August 2007, low SSTs, which were 5°C cooler than those off the coast, appeared along the coast from 35° N to 36° N and spread out across the region beyond 36° N (Figure 7(*a*)). In late August, SSTs seemed to have been advected to the northeast (Figure 7(*b*)). The SST image was partly obscured by clouds, but those along-coast low SSTs were comparatively matched with the region where a low magnitude of SAR-derived wind speeds was apparent. This implied that the spatial distinction of coastal winds was mostly related to variations in SST at the coastal area.

Moreover, it is known that the southeasterly wind blows predominantly from July to August along the east coast of Korea (Lee 1983; Lee and Na 1985). This year, stronger southerly winds blew longer than previous years (Park and Kim 2010). As shown in Figure 8, the time series of *in situ* wind measurements from KMA AWS indicates that southerly wind, which tends to induce coastal upwelling in the Northern Hemisphere, was dominant throughout August 2007. Significant southerly winds of magnitudes greater than 6 m s$^{-1}$ blew over two periods from 1 to 17 August and partly from 20 to 26 August, with cold water masses appearing after a time lag of approximately 1−3 days. It seems to be typical of the pattern of wind-induced upwelling events prevalent in the region (Lee and Na 1985; Suh, Jang, and Hwang 2001; Lee, Kim, and Kim 2003; Kim and Kim 2008), although this particular duration was longer than the average year. *In situ* SST measurements from the NFRDI coastal station demonstrated that SSTs along the coast started to decrease drastically from early August and lasted to nearly the end of the month, until the magnitude of southerly winds began to decrease to less than 2 m s$^{-1}$. Thus, the spatial distinctions of wind speeds associated with coastal upwelling were apparent on SAR-derived high-resolution wind fields.
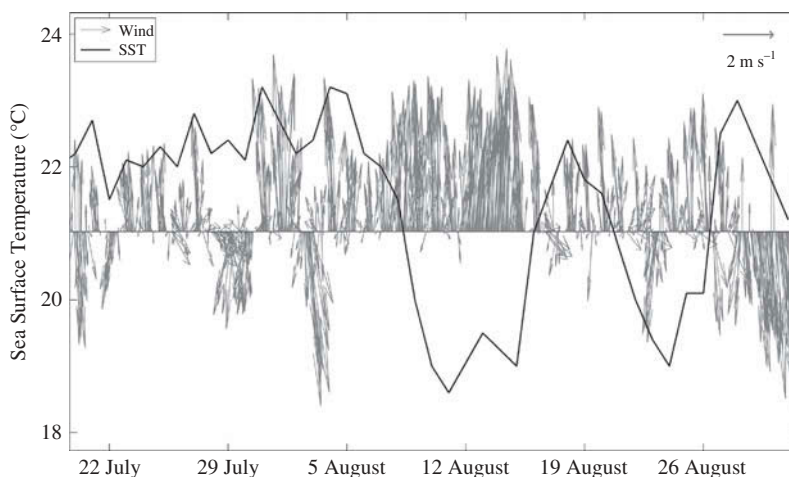
Figure 8.   Time series of wind vector (grey arrow, m s$^{-1}$) from AWS measurement of KMA and sea-surface temperature (black solid, °C) from NFRDI coastal station measurements.

### 4.3.   Stability effect on wind speed

Figures 6(*a*) and (*b*) clearly show small NRCS values in the upwelling zones off the coast, which were contrasted by high NRCS offshore regions. There have been several arguments as to whether the low wind speeds corresponding to small NRCSs were induced by low temperatures due to upwelled cold water or atmospheric stability within the MABL. Clemente-Colon and Yan (1999) addressed the effect of changes in MABL stability and viscous properties of the sea surface on the variation of NRCS. Other researches have pointed out that the upwelled cold water has an effect on the initiation and dissipation of short gravity waves, which in turn leads to a decrease in radar backscattering and hence the magnitude of wind speeds (Weissman 1990; Zheng et al. 1995).

To distinguish between the different effects on satellite measurements, we estimated changes in NRCS values and compared them with the dependence of radar backscattering on water viscosity based on the method of Zheng et al. (1995). The backscattering attenuation gradient of the section in Figure 7(*a*) has a much larger gradient of about 1.2 dB °C$^{-1}$ than the threshold of 0.217 dB °C$^{-1}$ set by Zheng et al. (1995). Such a large difference implies that the attenuation gradient of NRCS was mainly induced by other additional factors. It has been reported that the sensitivity of the NRCS to SST, which is related to changes in the marine boundary layer stability, is estimated to be up to 1−2 dB °C$^{-1}$ based on analysis of the US east coast upwelling feature (Clemente-Colón 2001; Donato and Marmorino 2002). Thus, it is inferred that the low wind speeds at the present upwelling region were caused by the modification of wind fields due to changes in MABL stability.

The stability of MABL can be indirectly estimated by the air–sea temperature difference. Figure 9(*a*) presents a comparison of temperature difference (°C) between SST and air temperature, $T_s - T_a$, and retrieved wind speed from the ALOS PALSAR image along the section in Figure 7(*a*). For the analysis of wide coverage, air temperature data from the ECMWF reanalysis data was used. A value of $T_a$ including the cross-section was about 25.1°C, which was similar to the 10 year average (24.5°C) of *in situ* measurements observed from 2001 to 2010 at the NFRDI coastal station (35.49° N, 129.44° E).
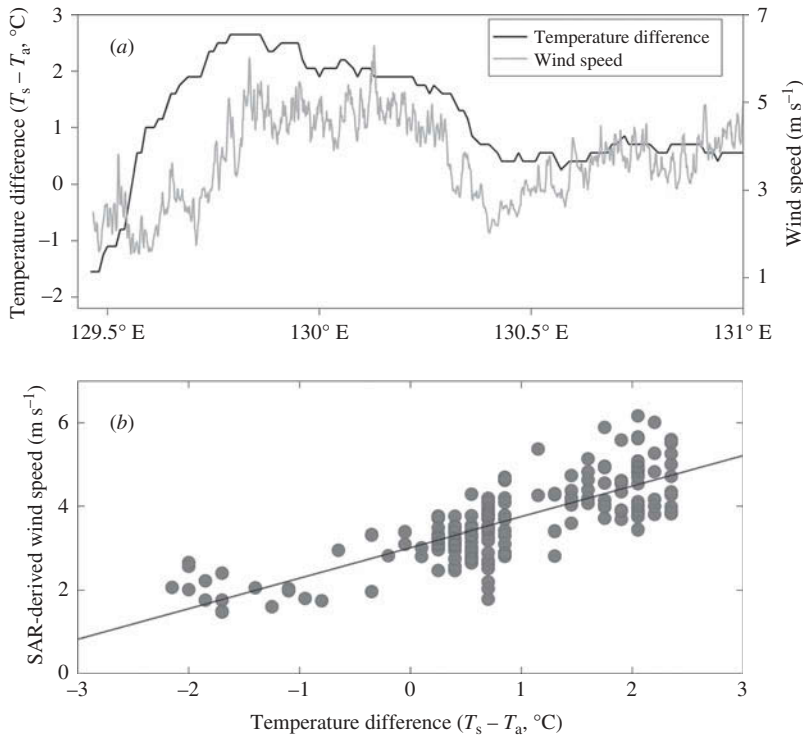
Figure 9.   (a) Comparison of sea-surface temperature (ºC) and SAR-derived wind speed (m s$^{-1}$) along 35.6º N (<131º E) as shown in the blue line of Figure 7 and (b) SAR-derived wind speeds as a function of temperature difference (ºC) between sea-surface temperature ($T_s$) and air temperature ($T_a$).

As shown in Figure 7(a), wind speed ranged from 1.5 to 6.3 m s$^{-1}$ and the SST–air temperature difference ranged from −1.7ºC to 2.1ºC. It is indeed, however, assumed that actual SST at the upwelling event was much lower than those from satellite observation. When strong upwelling occurs, the coastal region is frequently covered with clouds and fogs overall so that it is difficult to observe low temperature at the time from satellite SST images (Clemente-Colon and Yan 1999; Uiboupin and Laanemets 2009). According to previous research, when the cold water mass induced by coastal upwelling appeared, SST at this region dropped to 11–16 ºC (Lee and Na 1985; Suh, Jang, and Hwang 2001; Lee, Kim, and Kim 2003; Kim et al. 2010; Park and Kim 2010). Despite that, when compared to those at non-upwelling regions, the surface layer at the coastal region can be regarded as a relatively stable state. This implies that the effect of MABL stability induced the modification of the derived wind field in this region. As the marine-atmospheric boundary layer becomes more destabilized (stabilized), higher (less) momentum can be transferred, i.e. increasing (decreasing) wind stress, and thus amplifying (reducing) the magnitude of surface winds (Park, Cornillon, and Codiga 2006). Johannessen et al. (1996) also demonstrated that the variation of the radar backscattering near coastal fronts is attributed to the change in MABL stability under large air–sea temperature differences analogous to those of the study area.

Figure 9(b) illustrates that wind speed magnitude has an obvious positive correlation with the difference between SST and air temperature ($R^2 = 0.63$). The wind speed tends to increase at a rate of 0.73 m s$^{-1}$ ºC$^{-1}$ as the temperature difference increases. As the

difference between SST and surface air temperature increases, the instability of MABL increases. As MABL becomes more destabilized, higher momentum can be transferred, i.e. increasing wind stress, and thus amplifying the magnitude of surface winds (Park, Cornillon, and Codiga 2006). Thus, the low wind speed of the upwelling zone is believed to have been induced by air–sea temperature differences and a change in MABL stability.

### 4.4. Biological impact of upwelling

The upwelling event along the east coast of Korea in the summer of 2007 was the strongest recorded during the past decades (Park and Kim 2010). It appeared from the southern part to the northern part over 37º N, which was much farther north than the usual upwelling sites as that in this study. While a cold water mass induced by upwelling was dominantly present at the southern part only in the normal upwelling period, the strong upwelling events in the summer of 2007 were present in both southern and northern coasts of Korea. Figures 10(*a*) and (*c*) present the distributions of SST, which indicate one of the typical upwelling patterns off the east coast of Korea (Figure 10(*a*)) and the distinct feature of upwelling after its predominant period from late July to early August 2007 (Figure 10(*c*)), respectively. In the case of the normal upwelling in 2006, a cold water mass induced by upwelling was dominantly present from 35.5−36.5° N, and advected northeastward within tens of kilometres from the coast. On the contrary, the characteristic strong southerly winds were dominant in the summer of 2007, so that favourable conditions for upwelling maintained longer in this region. As a result, a cold band of water appeared along the coast from 36° N to 37.5° N, over 100 km north from the common upwelling site, and advected eastward much farther from the coast. The flow of advected cold water induced by upwelling formed significantly strong fronts corresponding to the flow of the second branch of the Tsushima Warm Current (Figure 10(*c*)). The spatial
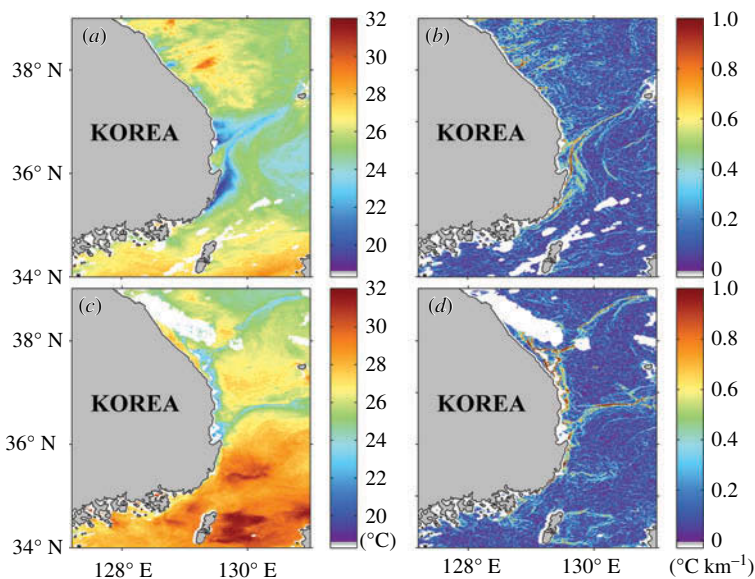


Figure 10. Distributions of sea-surface temperature (°C) and its gradient (°C km$^{-1}$) on 1 August 2006 ((*a*) and (*c*)) and 17 August 2007 ((*b*) and (*d*)), respectively.
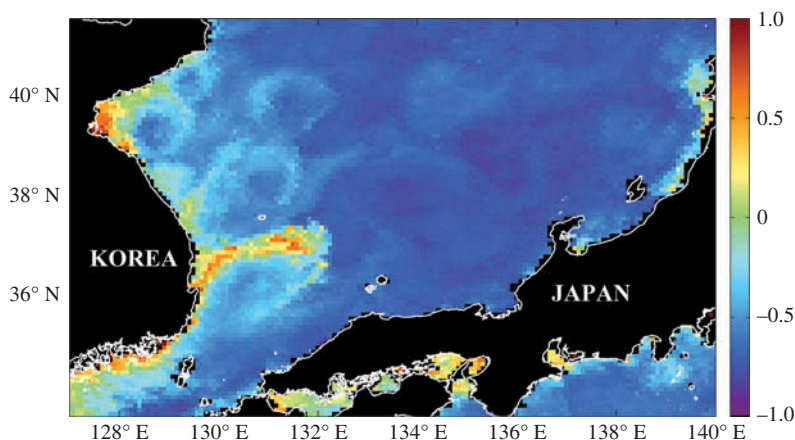
Figure 11. Distribution of monthly averaged chlorophyll-*a* concentration ($\log_{10}$ mg m$^{-3}$) from SeaWiFS in the East/Japan Sea in August 2007.

distribution of SST gradients also revealed the eastward advection of low cold waters with a large spatial gradient greater than 0.5°C km$^{-1}$ as shown in Figures 10(*b*) and (*c*).

Moreover, phytoplankton blooms on the coastal ocean surface were invoked by upwelling. The blooms of phytoplankton are highly dependent on the surrounding environmental conditions. The upwelling brings nutrient-rich water with low temperature from the deep ocean. Since the light conditions for photosynthesis are normally favourable in the summer, the supply of nutrients by upwelling may be one of the most important factors in controlling the phytoplankton blooms. Figure 11 shows the distribution of chlorophyll-*a* concentration from SeaWiFS data in the EJS during August 2007. The feature of the bloom extended to the northeast and then to the east, which was quite similar to the SST patterns shown in Figure 10(*c*). This supports our hypothesis on the bloom related to upwelling, cold water, and nutrients. As the upwelling activities become increasingly sustained, so too will the blooms be enhanced and subsequently advected offshore.

## 5. Summary and conclusion

To identify the relationship between the modification of SAR-derived coastal wind data and upwelling events along the east coast of Korea in the EJS, high-resolution coastal wind fields were retrieved from L-band SAR imagery. Comparison of the retrieved SAR wind speeds with *in situ* buoy wind measurements showed a small difference of less than 1 m s$^{-1}$, which implied that the results of SAR wind retrieval satisfied the limit of accuracy of satellite scatterometry.

The SAR-derived wind fields presented the detailed structure of wind fields along the coastal areas, which had heretofore been unobtainable from scatterometer observation. The retrieved SAR wind fields off the east coast of Korea during August 2007 showed the distinct patterns of low wind along the coastal region. The analysis of SAR wind fields with coincided SST images indicated that these spatial distinctions of SAR wind fields were associated with the upwelling events, which were induced by strong southerly winds in 2007. Based on wind and SST data from satellite data and *in situ* measurements, it was

found that significant wind-driven upwellings were prevalent in the summer, and that dominant low SSTs along the coastal region appeared to indicate a large difference of air–sea temperature, which reached around −6ºC.

The low wind speeds may be the result of changes in MABL stability or seawater viscosity. In most of the cases, however, it is difficult to determine which one is the major factor due to difficulty in distinguishing their contributions from one another. However, under the particular circumstance of large air–sea temperature differences, as in the study area, the variation of the radar backscattering near coastal fronts was much higher than the threshold suggested by previous literature. SAR data showed a large backscattering attenuation to SST ratio at the upwelling region, which was much greater than the dependence of water viscosity on radar backscattering, whereas the wind speed magnitude showed a positive correlation with the difference between SST and air temperature, which indirectly indicated MABL stability. The analysed results of SAR and SST data provide convincing evidence for this hypothesis. Therefore, it can be concluded that the changes in MABL stability caused by upwelling events dominantly generated the variation of SAR wind fields at the coastal regions.

The upwelling off the east coast of Korea in 2007 took place unprecedentedly due to long-term changes in the atmospheric environment, such as the North Pacific High and tropical depression. According to the previous literature, long-term changes in SST showed a negative trend, i.e. the cold water mass would appear more frequently and more strongly at the eastern coast of Korea including the present upwelling region. Moreover, the upwelling activities also induced a significant biological impact on the strong blooms in 2007. Thus, monitoring high-resolution sea-surface wind fields and SSTs will continue to increase in importance when it comes to understanding the process of upwelling and its connection to large-scale and remote forcings.

This study attempted to identify the causes of spatial distinctions among wind fields along the coastal region in the EJS, besides the physical and biological impacts of upwelling activity through multi-satellite observations. Usually coastal regions are frequently covered with clouds and fogs in the upwelling period so that it has long been difficult to observe the areas using optical or IR-sensored satellite observation. In this respect, using SAR data provides opportunities to investigate upwelling along the coastal region with its all-weather high-resolution imaging capability. Although it should be dealt with carefully in the interpretation of oceanic features on SAR image, it is anticipated that the applicability of SAR data with the use of other satellite observations and *in situ* measurements will contribute to our understanding of the characteristics of small-scale oceanographic phenomena, particularly at coastal areas without satellite scatterometer observations, as well as our further understanding of oceanic dynamics related to air–sea interaction at the sea surface and MABL dynamics.

# References

Bakun, A. 1990. "Global Climate Change and Intensification of Coastal Ocean Upwelling." *Science* 247 (4939): 198–201. doi:10.1126/science.247.4939.198.

Barth, J. A., and P. A. Wheeler. 2005. "Introduction to Special Section: Coastal Advances in Shelf Transport." *Journal of Geophysical Research* 110: C10S01. doi:10.1029/2005JC003124.

Bisagni, J. J., and M. H. Sano. 1993. "Satellite Observations of Sea Surface Temperature Variability on Southern Georges Bank." *Continental Shelf Research* 13: 1045–1064. doi:10.1016/0278-4343(93)90040-5.

Bourassa, M. A., D. G. Vincent, and W. L. Wood. 1999. "A Flux Parameterization Including the Effects of Capillary Waves and Sea State." *Journal of the Atmospheric Sciences* 56 (9): 1123–1139. doi:10.1175/1520-0469(1999)056<1123:AFPITE>2.0.CO;2.

Brown, R. A., and W. T. Liu. 1982. "An Operational Large-Scale Marine Planetary Boundary Layer Model." *Journal of Applied Meteorology* 21 (3): 261–269. doi:10.1175/1520-0450(1982)021<0261:AOLSMP>2.0.CO;2.

Businger, J. A., and W. J. Shaw. 1984. "The Response of the Marine Boundary Layer to Mesoscale Variations in Sea-Surface Temperature." *Dynamics of Atmospheres and Oceans* 8: 267–281. doi:10.1016/0377-0265(84)90012-5.

Businger, J. A., J. C. Wyngaard, Y. Izumi, and E. F. Bradley. 1971. "Flux–Profile Relationships in the Atmospheric Surface Layer." *Journal of the Atmospheric Sciences* 28: 181–189. doi:10.1175/1520-0469(1971)028<0181:FPRITA>2.0.CO;2.

Campbell, J. W., J. M. Blaisdell, and M. Darzi. 1995. "Level-3 SeaWiFS Data Products: Spatial and Temporal Binning Algorithms." In *NASA Technical Memorandum 104566*, edited by S. B. Hooker, E. R. Firestone, and J. G. Acker, 32, 73 p. Greenbelt, MD: NASA Goddard Space Flight Center.

Clemente-Colón, P. 2001. "Evolution of Upwelling-Associated Biological Features in the Middle Atlantic Bight as Captured by SAR, SST, and Ocean Color Sensors." *Proceedings of International Geoscience and Remote Sensing Symposium*, Sydney, July 9–13, vol. 6, 2616–2618. doi:10.1109/IGARSS.2001.978107.

Clemente-Colon, P., and X.-H. Yan. 1999. "Observations of East Coast Upwelling Conditions in Synthetic Aperture Radar Imagery." *IEEE Transactions on Geoscience and Remote Sensing* 37 (5): 2239–2248. doi:10.1109/36.789620.

Donato, T. F., and G. O. Marmorino. 2002. "The Surface Morphology of a Coastal Gravity Current." *Continental Shelf Research* 22 (1): 141–146. doi:10.1016/S0278-4343(01)00066-8.

Dyer, A. J. 1974. "A Review of Flux-Profile Relationships." *Boundary-Layer Meteorology* 7: 363–372. doi:10.1007/BF00240838.

Flament, P., L. Armi, and L. Washburn. 1985. "The Evolving Structure of an Upwelling Filament." *Journal of Geophysical Research* 90: 11765–11778. doi:10.1029/JC090iC06p11765.

Fragiacomo, C., and F. Parmiggiani. 2002. "An Upwelling Event in the Central Mediterranean Sea Detected by QuikSCAT and by AVHRR." *International Journal of Remote Sensing* 23 (24): 5151–5153. doi:10.1080/0143116021000016752.

Geernaert, G. L., and K. B. Katsaros. 1986. "Incorporation of Stratification Effects on the Oceanic Roughness Length in the Derivation of the Neutral Drag Coefficient." *Journal of Physical Oceanography* 16: 1580–1584. doi:10.1175/1520-0485(1986)016<1580:IOSEOT>2.0.CO;2.

Hooker, S. B., W. E. Esaias, G. G. Feldman, W. W. Gregg, and C. R. McClain. 1992. "An Overview of SeaWiFS and Ocean Color." In *NASA Technical Memorandum 104566*, edited by S. B. Hookerand and E. R. Fierstone, 1, 24 p. Greenbelt, MD: NASA Goddard Space Flight Center.

Hsu, M.-K., L. M. Mitnik, and C.-T. Liu. 1995. "Upwelling Area Northeast of Taiwan on ERS-1 SAR Images." *Acta Oceanographica Taiwanica* 34 (3): 27–38.

Isoguchi, O., and M. Shimada. 2009. "An L-Band Ocean Geophysical Model Function Derived from PALSAR." *IEEE Transactions on Geoscience and Remote Sensing* 47: 1925–1936. doi:10.1109/TGRS.2008.2010864.

Isoguchi, O., M. Shimada, and H. Kawamura. 2011. "Characteristics of Ocean Surface Winds in the Lee of an Isolated Island Observed by Synthetic Aperture Radar." *Monthly Weather Review* 139 (6): 1744–1761. doi:10.1175/2010MWR3564.1.

Johannessen, J. A., R. A. Shuchman, G. Digranes, D. R. Lyzenga, C. Wackerman, M. Johannessen, and P. W. Vachon. 1996. "Coastal Ocean Fronts and Eddies Imaged with ERS-1 Synthetic Aperture Radar." *Journal of Geophysical Research* 101 (C3): 6651–6667. doi:10.1029/95JC02962.

Kara, A. B., A. J. Wallcraft, and M. A. Bourassa. 2008. "Air-Sea Stability Effects on the 10 m Winds over the Global Ocean: Evaluations of Air-Sea Flux Algorithms." *Journal of Geophysical Research* 113: C4009. doi:10.1029/2007JC004324.

Kim, D.-S., and D.-H. Kim. 2008. "Numerical Simulation of Upwelling Appearance near the Southeastern Coast of Korea." *Journal of the Korean Society of Marine Environment and Safety* 14 (1): 1–7.

Kim, K., K. R. Kim, D. H. Min, Y. Volkov, J. H. Yoon, and M. Takematsu. 2001. "Warming and Structural Changes in the East (Japan) Sea: A Clue to Future Changes in Global Oceans?" *Geophysical Research Letters* 28 (17): 3293–3296. doi:10.1029/2001GL013078.

Kim, S.-W., W.-J. Go, S.-S. Kim, H.-D. Jeong, and K. Yamada. 2010. "Characteristics of Ocean Environment before and after Coastal Upwelling in the Southeastern Part of Korean Peninsula Using an In-Situ and Multi-Satellite Data." *Journal of the Korean Society of Marine Environment and Safety* 16 (4): 345–352.

Kim, T.-S., K.-A. Park, W.-M. Choi, S. Hong, B.-C. Choi, I. Shin, and K.-R. Kim. 2012. "L-Band SAR-Derived Sea Surface Wind Retrieval off the East Coast of Korea and Error Characteristics." *Korean Journal of Remote Sensing* 28 (5): 477–487. doi:10.7780/kjrs.2012.28.5.1.

Kim, T.-S., K.-A. Park, and W. Moon. 2010. "Wind Vector Retrieval from SIR-C SAR Data off the East Coast of Korea." *Journal of Korean Earth Science Society* 31 (5): 475–487. doi:10.5467/JKESS.2010.31.5.475.

Lathuilière, C., V. Echevin, and M. Lévy. 2008. "Seasonal and Intraseasonal Surface Chlorophyll-A Variability along the Northwest African Coast." *Journal of Geophysical Research* 113: C05007. doi:10.1029/2007JC004433.

Lee, D.-K., J.-I. Kwon, and S.-B. Hahn. 1998. "The Wind Effect on the Cold Water Formation near Gampo-Ulgi Coast." *Journal of the Korean Fisheries Society* 31 (3): 359–371.

Lee, H.-W., H.-E. Ji, and S.-H. Lee. 2009. "A Study of Interrelationships between the Effect of the Upwelling Cold Water and Sea Breeze in the Southeastern Coast of the Korean Peninsula." *Journal of Korean Society for Atmospheric Environment* 25 (6): 481–492. doi:10.5572/KOSAE.2009.25.6.481.

Lee, J. C. 1983. "Variations of Sea Level and Sea Surface Temperature Associated with Wind-Induced Upwelling in the Southeast Coast of Korea in Summer." *Journal of the Oceanological Society of Korea* 18: 149–160.

Lee, J. C. 2011. "Upwelling-Response of the Cold Water off Haeundae in Summer." *Journal of the Korean Society of Oceanography* 16 (4): 206–211.

Lee, J. C., D. H. Kim, and J.-C. Kim. 2003. "Observations of Coastal Upwelling at Ulsan in Summer 1997." *Journal of the Korean Society of Oceanography* 38 (3): 122–134.

Lee, J. C., and J. Y. Na. 1985. "Structure of Upwelling off the Southeast Coast of Korea." *Journal of the Oceanological Society of Korea* 20 (3): 6–19.

Leite, G. C., D. M. Ushizima, F. N. S. Medeiros, and G. G. de Lima. 2010. "Wavelet Analysis for Wind Fields Estimation." *Sensors* 10: 5994–6016. doi:10.3390/s100605994.

Li, X. M., X. F. Li, and M. X. He. 2009. "Coastal Upwelling Observed by Multi-Satellite Sensors." *Science in China Series D: Earth Sciences* 52 (7): 1030–1038. doi:10.1007/s11430-009-0088-x.

Liu, W. T. 1984. "The Effects of the Variations in Sea Surface Temperature and Atmospheric Stability in the Estimation of Average Wind Speed by SEASAT-SASS." *Journal of Physical Oceanography* 14: 392–401. doi:10.1175/1520-0485(1984)014<0392:TEOTVI>2.0.CO;2.

Liu, W. T., K. B. Katsaros, and J. A. Businger. 1979. "Bulk Parameterization of Air-Sea Exchanges of Heat and Water Vapor Including the Molecular Constraints at the Interface." *Journal of the Atmospheric Sciences* 36: 1722–1735. doi:10.1175/1520-0469(1979)036<1722:BPOASE>2.0.CO;2.

Liu, W. T., and W. Tang. 1996. *Equivalent Neutral Wind*, 8 p. JPL Publication 96-17. Pasadena, CA: NASA Jet Propulsion Laboratory.

Marín, V. H., L. E. Delgado, and R. Escribano. 2003. "Upwelling Shadows at Mejillones Bay (Northern Chilean Coast): A Remote Sensing, in Situ Analysis." *Investigaciones Marinas* 31 (2): 47–55. doi:10.4067/S0717-71782003000200005.

McClain, C. R., L. J. Pietrafesa, and J. A. Yoder. 1984. "Observations of Gulf Stream-Induced and Wind-Driven Upwelling in the Georgia Bight Using Ocean Color and Infra-Red Imagery." *Journal of Geophysical Research* 89: 3705–3723. doi:10.1029/JC089iC03p03705.

McClain, E. P., W. G. Pichel, and C. C. Walton. 1985. "Comparative Performance of Avhrr-Based Multichannel Sea Surface Temperatures." *Journal of Geophysical Research* 90 (C6): 11587–11601. doi:10.1029/JC090iC06p11587.

Nykjaer, L., and L. Van Camp. 1994. "Seasonal and Interannual Variability of Coastal Upwelling along Northwest Africa and Portugal from 1981 to 1991." *Journal of Geophysical Research* 99 (C7): 14197–14207. doi:10.1029/94JC00814.

Park, K.-A., P. Cornillon, and D. L. Codiga. 2006. "Modification of Surface Winds near Ocean Fronts: Effects of Gulf Stream Rings on Scatterometer (QuikSCAT, NSCAT) Wind Observations." *Journal of Geophysical Research* 111: C03021. doi:10.1029/2005JC003016.

Park, K.-A., and K.-R. Kim. 2010. "Unprecedented Coastal Upwelling in the East/Japan Sea and Linkage to Long Term Large Scale Variations." *Geophysical Research Letters* 37. doi:10.1029/2009GL042231.

Paulson, C. A. 1970. "The Mathematical Representation of Wind Speed and Temperature Profiles in the Unstable Atmospheric Surface Layer." *Journal of Applied Meteorology* 9 (6): 857–861. doi:10.1175/1520-0450(1970)009<0857:TMROWS>2.0.CO;2.

Peixoto, J. P., and A. H. Oort, eds. 1992. *Physics of Climate*, 520 p. Woodbury, NY: American Institute of Physics.

Pradhan, Y., S. J. Lavender, N. J. Hardman-Mountford, and J. Aiken. 2006. "Seasonal and Inter-Annual Variability of Chlorophyll-A Concentration in the Mauritanian Upwelling: Observation of An Anomalous Event during 1998–1999." *Deep Sea Research Part II: Topical Studies in Oceanography* 53: 1548–1559. doi:10.1016/j.dsr2.2006.05.016.

Santos, A. M. P., A. S. Kazmin, and Á. Peliz. 2005. "Decadal Changes in the Canary Upwelling System As Revealed by Satellite Observations: Their Impact on Productivity." *Journal of Marine Research* 63 (2): 359–379. doi:10.1357/0022240053693671.

Shimada, M., H. Nakatani, K. Isono, and T. Kawada. 1999. "Removal of the Interference Appeared within the SAR Images." *Advances in Space Research* 23: 1505–1508. doi:10.1016/S0273-1177(99)00304-X.

Smith, R. L. 1968. "Upwelling." In *Oceanography and Marine Biology – An Annual Review, Vol. 6*, edited by H. Barnes, 11–46. London: George Allen and Unwin.

Suh, Y. S., L.-H. Jang, and J. D. Hwang. 2001. "Temporal and Spatial Variations of the Cold Waters Occurring in the Eastern Coast of the Korean Peninsula in Summer Season." *Korean Journal of Fisheries and Aquatic Sciences* 34 (5): 435–444.

Svejkovsky, J., and J. Shandley. 2001. "Detection of Offshore Plankton Blooms with AVHRR and SAR Imagery." *International Journal of Remote Sensing* 22 (2–3): 471–485. doi:10.1080/014311601450040.

Thomas, A. C., J. L. Blanco, M. E. Carr, P. T. Strub, and J. Osses. 2001. "Satellite-Measured Chlorophyll and Temperature Variability off Northern Chile during the 1996–1998 La Niña and El Niño." *Journal of Geophysical Research* 106 (C1): 899–915. doi:10.1029/1999JC000052.

Uiboupin, R., and J. Laanemets. 2009. "Upwelling Characteristics Derived from Satellite Sea Surface Temperature Data in the Gulf of Finland, Baltic Sea." *Boreal Environment Research* 14: 297–304.

Vachon, P., and F. Dobson. 2000. "Wind Retrieval from RADARSAT SAR Images: Selection of a Suitable C-Band HH Polarization Wind Retrieval Model." *Canadian Journal of Remote Sensing* 26: 306–313.

Van Camp, L., L. Nykjaer, E. Mittelstaedt, and P. Schlittenhardt. 1991. "Upwelling and Boundary Circulation off Northwest Africa as Depicted by Infrared and Visible Satellite Observations." *Progress in Oceanography* 26 (4): 357–402. doi:10.1016/0079-6611(91)90012-B.

Wackerman, C., C. Rufenach, R. Schuchman, J. Johannessen, and K. Davidson. 1996. "Wind Vector Retrieval Using ERS-1 Synthetic Aperture Radar Imagery." *Journal of Geophysical Research* 34: 1343–1352.

Weissman, D. E. 1990. "Dependence of the Microwave Radar Cross Section on Ocean Surface Variables: Comparison of Measurements and Theory Using Data from the Frontal Air-Sea Interaction Experiment." *Journal of Geophysical Research* 95 (C3): 3387–3398. doi:10.1029/JC095iC03p03387.

Willson, H. R., and N. W. Rees. 2000. "Classification of Mesoscale Features in the Brazil-Falkland Current Confluence Zone." *Progress in Oceanography* 45: 415–426. doi:10.1016/S0079-6611(00)00011-2.

Zheng, Q., X.-H. Yan, V. Klemas, C. Ho, N. Kuo, and Z. Wang. 1998. "Coastal Lee Waves on ERS-1 SAR Images." *Journal of Geophysical Research* 103 (C4): 7979–7993. doi:10.1029/97JC02176.

Zheng, Q., X.-H. Yan, V. Klemas, N. E. Huang, J.-Y. Pan., and Y.-I. Yuan. 1995. "Laboratory Measurements of the Effects of Viscosity on Short Water Wave Spectra and Implication for Radar Remote Sensing of the Ocean Surface." *Chinese Journal of Oceanology and Limnology* 13 (3): 193–205. doi:10.1007/BF02850519.